Time-Domain Parameter Extraction Method for Thévenin-Equivalent Circuit Battery Models

Ari Hentunen, *Member, IEEE*, Teemu Lehmuspelto, *Member, IEEE*, and Jussi Suomela

***Abstract*—This paper presents an analytical time-domain-based parameter identification method for Thévenin-equivalent circuit-based lithium-ion battery models. The method is based on the analysis of voltage-relaxation characteristics of pulse discharge and pulse charge experiments, and the method can be used for both discharge and charge operation with any number of parallel resistor-capacitor branches. The use of the method is demonstrated for a second-order model and validated with a real-world duty cycle. Experimental results for a commercial lithium-ion battery module are presented.**

***Index Terms*—Batteries, battery management systems (BMSs), electric vehicles (EVs), equivalent circuits, parameter extraction.**

I. Introduction

THE interest in vehicle electrification has been rising steadily as we are moving toward sustainable transportation. Due to increased demand from customers and maturing technology, automobile manufacturers are now introducing electric vehicles (EVs), such as battery EVs, hybrid EVs, and plug-in hybrid EVs in increasing pace. Also, heavy vehicle and non-road mobile machinery industries have shown rising interest to electrify the drive train. The driving forces are the remarkably tightening legislation and regulations for the exhaust emissions of the diesel engines used in NRMM, the desire to improve performance, safety, and operator comfortability, and the desire to decrease operating cost. Common for all EVs is that a large electrochemical battery is used as an energy storage to power the vehicle. Lithium-ion (Li-ion) chemistries offer superb properties such as high power rating, high energy density, and high cycle life, and therefore, they are likely to be largely adopted by EV manufacturers [1].

In the early stages of a vehicle electrification development, simulations are usually used as a tool to evaluate concept studies and to validate early design goals. As the development process goes on, more accurate models of subsystems are needed to validate the component selection and sizing as well as to provide information for vehicle's control algorithms. Accurate and computationally light battery models are needed for these simulations. Accurate battery models accompanied with parameter adaptation algorithms are also needed in certain real-time applications, e.g., in battery management systems (BMSs), to estimate important quantities such as state of charge (SOC), state of health, and available power [2].

Modeling of electrochemical batteries is challenging due to their high level of nonlinearity. The characteristics such as impedance are, in general, nonlinear multivariable functions of the SOC, temperature, aging, current direction, and rate. There are several different kinds of modeling approaches, which can be generally divided into electrochemical [3], mathematical [4], and electrical [5]–[7] modeling. Lately, also models that combine mathematical and electrical models have been introduced (e.g., [8]). For system-level simulations of EVs, Thévenin-based [6] or impedance-based [7] electrical models are commonly used, because they are fast to execute, simple and intuitive to analyze, and provide accurate SOC, open-circuit voltage (OCV), and terminal voltage prediction under dynamic load current profile [9]. The model can be augmented to predict also the temperature [10], which is often needed in the simulations. Due to inherent simplicity of electrical models, they can also be transformed into online models, which run inside a BMS [11].

The main difference between the impedance-based and Thévenin-based modeling methods is that the parameters of impedance-based models are extracted based on electrochemical impedance spectroscopy measurements in frequency domain [7], while Thévenin-based models are parameterized typically by (CP) experiments in time domain [12], i.e., experimental current and voltage time-series data. Thévenin-based models are attractive, because no impedance measurements need to be done. In addition, also battery modules and packs can be characterized and modeled directly based on the data from a battery cycler during performance tests of a battery module or pack. The basic experiments at the typical temperature and rate can be done in a couple of days [13]. If also the temperature and current-rate effects need to be extracted, the duration of the tests increases accordingly.

The Thévenin-based electrical model of [6] is commonly used for Li-ion battery modeling. The voltage response to current excitation is modeled as a Thévenin equivalent circuit, which is represented in Fig. 1, where s_Q is the SOC, u_{oc} is the OCV, u_{b} is the terminal voltage, i_{b} is the terminal current, R_0 is the ohmic resistance, $R_1, \ldots, R_n$ are the dynamic resistances, and $C_1, \ldots, C_n$ are the corresponding dynamic capacitances. All resistances and capacitances are functions of the SOC,

Manuscript received November 13, 2012; revised March 5, 2014; accepted April 10, 2014. Date of publication May 7, 2014; date of current version August 18, 2014. This work was carried out in the HybLab and ECV projects funded by the Multidisciplinary Institute of Digitalization and Energy (MIDE) of Aalto University and Finnish Funding Agency for Technology and Innovation (Tekes). Paper no. TEC-00592-2012.

A. Hentunen is with the Department of Electrical Engineering and Automation, School of Electrical Engineering, Aalto University, 02015 Espoo, Finland (e-mail: ari.hentunen@aalto.fi).

T. Lehmuspelto is with the Department of Engineering Design and Production School of Engineering, Aalto University, 02015 Espoo, Finland (e-mail: teemu.lehmuspelto@aalto.fi).

J. Suomela is with Hybria Oy, 02150 Espoo, Finland (e-mail: jussi.suomela@hybria.fi).

Color versions of one or more of the figures in this paper are available online at http://ieeexplore.ieee.org

Digital Object Identifier 10.1109/TEC.2014.2318205

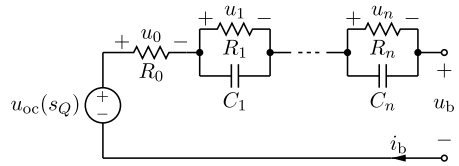

Fig. 1. Electrical equivalent circuit.

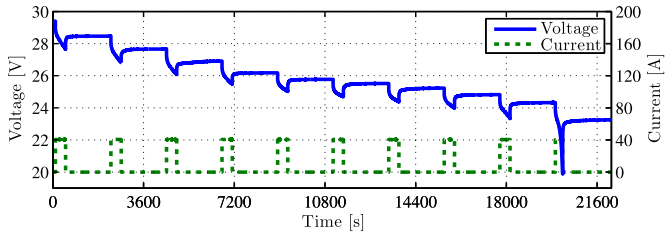

Fig. 2. Illustration of a PD experiment for a battery module.

temperature, rate, current direction, calendar life, and cycle life. The voltage source provides the predicted OCV as a function of the SOC. Generally, also temperature dependence and hysteresis effect can be included into the OCV prediction.

The number of resistor-capacitor (*RC*) branches depends on the desired accuracy and bandwidth of the model [14]. One to three branches are typically used. One *RC* branch is enough for early simulations of EVs. It is, however, often found that more branches are needed for more detailed simulations, vehicle software development, or BMS development [10], [11], [15]–[17]. The parameterization of one *RC* branch model is straightforward. However, the lack of systematic offline parameter identification methods for multiple *RC* branches has yield into use of ad hoc methods and iterative numerical optimization methods to parameterize the model.

The parameters for a first-order model can be predicted analytically from a short CP [12] or from the voltage relaxation after a CP has ended [13]. With some restrictions, the CP method [12] can also be applied for two *RC*-circuits. However, due to short duration of the CP, the shorter time constant is in the order of less than a second and the longer time constant is in the order of tens of seconds. These are too short time constants for system-level simulation of many battery systems, including EV applications. The analytical method of Hu *et al.* [17] can be applied for multiple-order models. However, it is limited for discharge operation. In addition, if the parameters are identified from the data during the load current, as in [12] and [17], then the SOC and OCV do not stay constant during the identification, which causes error to the parameters.

Most of the presented parameter identification methods for Thévenin-based models are based either on online parameter identification (e.g., [10], [11], [16], [18], [19]) or on iterative numerical optimization (e.g., [8], [9], [20], [21]). Online methods are not directly applicable for offline simulations. Iterative methods such as genetic algorithms and nonlinear least squares typically need initial guesses and have a high number of parameters to be identified, and thus, those methods are very sensitive for initial conditions, they may end up in a local minimum, and they may have numerical problems with convergence. They also need excessive iterative simulations to identify the parameters accurately and may need a lot of effort to find a good set of parameters. Thus, the identification process of iterative brute force methods may be very tedious and time intensive.

A simple and fast analytical time-domain-based method for *RC* circuit parameter extraction of Thévenin equivalent circuit battery models is presented in this paper. The method is based on the analysis of voltage relaxation characteristics of pulse discharge (PD) and pulse charge (PC) experiments, and the method can be used for both discharge and charge operation with any number of parallel *RC* branches. The computational burden of the proposed method remains low even if long rest times and high sampling frequency were used in the experiments. With the presented method, the parameter extraction can be done systematically and it can be easily automated. The use of the method is demonstrated and validated with experiments with a commercial 40 Ah Li-ion battery module. The presented parameter extraction method is not limited to automotive applications, but it can be applied to other applications and battery chemistries as well.

II. Model Extraction

The proposed *RC* parallel circuit identification method is based on the analysis of the voltage relaxation characteristics during the rest-times of the experimental PD and PC characterization tests. These PD and PC tests consist of a sequence of constant CPs with a rest time between pulses. The experiments should cover the typical rates of the anticipated load profile to provide accurate results. The duration of rest times and the number of pulses are both compromises of the desired accuracy and test duration. Rest times between 5 and 60 min and pulse rates between 2% and 20% are typically used. Fig. 2 illustrates a PD sequence at 1C rate, 10% pulse rate, and 30-min rest time. Each PD or PC test sequence characterizes the whole SOC range systematically. The starting times and ending times of the CPs are first identified, and the data are split accordingly into sections. Each rest time is analyzed separately. The rest period under investigation is then partitioned into separate time windows, which are used to identify the corresponding model parameters.

The parameters are typically scheduled for the SOC, temperature, and rate. Two parameter sets are identified, one for discharging, i.e., for positive current, and one for charging, i.e., for negative current. The resulting parameter mappings can be implemented, e.g., as mathematical functions or multidimensional look-up table.

The SOC must be tracked in order to make the SOC-scheduling. The SOC is defined as the ratio of the available charge to the usable charge capacity:

$$s_Q = \frac{Q}{Q_{\mathrm{us}}} \tag{1}$$

where s_Q is the SOC, Q is the available charge in the battery, and Q_{us} is the usable charge capacity of the battery. In (1), the

variable for the SOC is dimensionless and has a range of 0–1. It is also common to express it in percents. The SOC can be tracked, e.g., by the coulomb-counting method [6]:

$$s_Q = s_{Q\,0} - \frac{1}{Q_{\rm us}} \int i_{\rm b}\, dt \tag{2}$$

where $s_{Q\,0}$ is the initial SOC, and $i_{\rm b}$ is the battery current. It is recommended to first measure the real capacity and use it instead of the nominal capacity, if the values differ noticeably.

The ohmic resistance R_0 can be easily identified at the time-instants when a CP is beginning or ending:

$$R_0 = \left| \frac{\Delta U}{\Delta I} \right| \tag{3}$$

where ΔU is the instantaneous voltage difference during the current step, and ΔI is the amplitude of the current step.

For a model with *n*th order, the following time-domain equation represents the terminal voltage during a rest time after a CP has ended:

$$u_{\rm b} = u_{\rm oc} - \sum_{i=1}^{n} U_i\, {\rm e}^{-\frac{t}{\tau_i}} \tag{4}$$

where U_i is the initial voltage of the *i*th *RC* parallel branch and $\tau_i = R_i C_i$ is the corresponding time constant. The *RC* parallel branches model the activation polarization or charge-transfer overvoltage and concentration polarization at anode and cathode [22]. During rest time, the terminal voltage of a battery approaches OCV as the polarization decreases, finally reaching equilibrium. In (4), the *RC* branches voltages decrease with decay rates determined by the time constants τ_i, and eventually the battery voltage equals the OCV.

During a rest period of a PD or PC test, the transient circuit voltage, i.e., the total voltage over the resistor-capacitor network of the (EEC) of Fig. 1, can be expressed as

$$u_\tau(t) = U_{\rm oc} - u_{\rm b}(t) \tag{5}$$

where $U_{\rm oc}$ is the OCV, which stays constant during the rest period, and $u_{\rm b}(t)$ is the battery voltage as a function of time. Assuming that the rest time is sufficiently long so that the voltage reaches steady state, the OCV can be identified by taking the final voltage value at the end of each rest time. If shorter rest times are employed, other methods for the OCV-identification are recommended. Rapid methods are presented in [13].

Even though the transient circuit voltage of (5) is not a real measurable quantity and cannot be measured directly during the experiment, it can be obtained *a posteriori* from the data. By assuming the model structure of Fig. 1, the transient circuit voltage during a rest period can be represented as

$$u_\tau(t) = \sum_{i=1}^{n} U_i\, {\rm e}^{-\frac{t}{\tau}i} \tag{6}$$

where U_i is the initial voltage of the *i*th *RC* branch and τ_i is the corresponding time constant. For PD and PC experiments, the transient circuit voltage u_τ and all of the initial voltages U_i have always the same sign, i.e., positive for discharge and negative for charge when discharge is defined as positive current direction

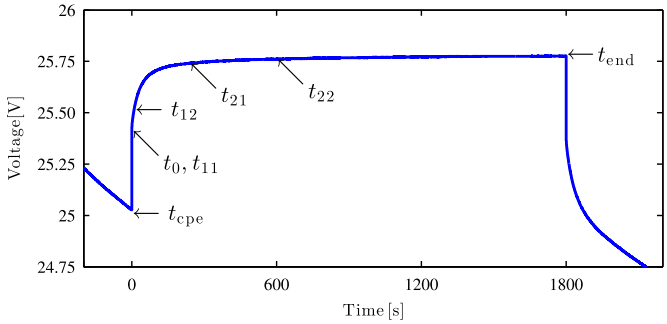

Fig. 3. Voltage relaxation characteristics during a PD test. Example time instants for two time windows are also shown. Time axis has been shifted to have origin at the beginning of rest time, i.e., t_0.

as in Fig. 1. The beginning time of the rest period should be extracted to be the time instant when the current reaches zero, i.e., right after the instantaneous voltage step caused by the ohmic resistance. The ending time instant should be extracted to be the time instant right before the next CP begins. The parameters U_i and τ_i can then be estimated from the transient circuit voltage u_τ data.

Let us use two *RC* circuits as a minimal example to demonstrate the full capabilities of the model extraction method. One *RC* circuit is then a special case of the presented method. For two *RC* branches, (6) becomes

$$u_\tau(t) = U_1\, {\rm e}^{-\frac{t}{\tau_1}} + U_2\, {\rm e}^{-\frac{t}{\tau_2}}. \tag{7}$$

Next, the rest period is divided into two partitions, which are used for parameter extraction of short and long time-constant branches, respectively. If more *RC* branches were used in the model structure, the rest period would need to be divided into as many partitions as there were *RC* circuits. Let us first define the time instants:

1) $t_{\rm cpe}$ is the time instant when the CP ends and current starts to fall.
2) t_0 is the time instant when the current has fallen back to zero, i.e., the beginning of rest time. In the following, this will be referred as $t = 0$ s.
3) t_{11} is the starting time of the first time window, typically $t_{11} = t_0$.
4) t_{12} is the ending time of the first time window.
5) t_{21} is the starting time of the second time window.
6) t_{22} is the ending time of the second time window.
7) $t_{\rm end}$ is the ending time of the rest period.

The partitioning of one rest time is illustrated in Fig. 3. Time windows should have a time gap between them, during which the voltage of the shorter time constant branch should fall very close to zero. This will be illustrated later in an example. The natural starting time for the first time window is t_0, i.e., $t = 0$ s. The starting time for the second time window should be later than three times the shorter time constant. This condition confirms that the voltage of the shorter time-constant branch has dropped below 5% of its initial value, and thus, it has only a negligible effect on the parameter extraction of the long time-constant branch. However, because the predicted time constants cannot

be known exactly before the parameter extraction, this condition should be checked afterward.

Let us start with the latter partition and choose the time instants t_{21} and t_{22} as its starting and ending time instants. This time window is now used to extract the long time-constant characteristics. It is first assumed that the two time constants are of different time scales, i.e., one is in the order of tens of seconds and the other is in the order of minutes or tens of minutes. It is also assumed that at the beginning of the second time window the fast time-constant voltage has dropped to zero. Then, the following expression can be written:

$$u_\tau(t) = u_\tau(t_{21})\,\mathrm{e}^{-\frac{t-t_{21}}{\tau_2}} \quad \text{for } t \geq t_{21}, \tag{8}$$

where the $u_\tau(t_{21})$ is the voltage at the starting time of the second time window. By setting the time as the ending time of the time window, i.e., $t = t_{22}$, the time constant τ_2 can be solved:

$$\hat{\tau}_2 = \frac{t_{22} - t_{21}}{\ln\left(\dfrac{u_\tau(t_{21})}{u_\tau(t_{22})}\right)} \quad \text{for } u_\tau \neq 0 \tag{9}$$

where a hat is used to denote predicted quantities to distinct them from the measured quantities.

The above equation works for both current directions, i.e., for both the PD and PC experiments, because the possible minus signs of the voltages cancel each other. It should be noted, however, that after a very long rest time, the transient circuit voltage approaches zero, which is not allowed. Therefore, the ending-time for the determination of the time constant should be selected appropriately so that the transient circuit voltage is not very close to zero. The initial voltage of the second branch at time instant t_0 can then be obtained:

$$\hat{U}_2 = u_\tau(t_{21})\,\mathrm{e}^{\frac{t_{21}}{\tau_2}}. \tag{10}$$

The predicted voltage of the second *RC* branch can then be expressed as

$$\hat{u}_2(t) = \hat{U}_2\,\mathrm{e}^{-\frac{t}{\tau_2}} \quad \text{for } t \geq 0. \tag{11}$$

After U_2 and τ_2 have been obtained, the first time window can be used to extract the parameters of the short time-constant *RC* branch. Those parameters can be extracted the same way as for the second time window, but the data must be first preprocessed by subtracting the predicted long time-constant branchs voltage from the experimental data:

$$u'_\tau(t) = u_\tau(t) - \hat{u}_2(t) = U_{\mathrm{oc}} - u_{\mathrm{b}}(t) - \hat{u}_2(t) \tag{12}$$

where an apostrophe denotes altered voltage after the subtraction of the predicted long time-constant voltage. The altered transient circuit voltage can be expressed as

$$u'_\tau(t) = u'_\tau(t_{11})\,\mathrm{e}^{-\frac{t-t_{11}}{\tau_1}} \quad \text{for } t \geq t_{11} \tag{13}$$

where the $u'_\tau(t_{11})$ is the voltage of the altered transient circuit voltage at the starting time of the first time window. Then, the time constant can be solved:

$$\hat{\tau}_1 = \frac{t_{12} - t_{11}}{\ln\left(\dfrac{u'_\tau(t_{11})}{u'_\tau(t_{12})}\right)} \quad \text{for } u'_\tau \neq 0. \tag{14}$$

The initial voltage of the first branch at time instant t_0 can then be obtained as follows:

$$\hat{U}_1 = u'_\tau(t_{11})\,\mathrm{e}^{\frac{t_{11}}{\tau_1}}. \tag{15}$$

The predicted voltage of the first *RC* branch can be written as

$$\hat{u}_1(t) = \hat{U}_1\,\mathrm{e}^{-\frac{t}{\tau_1}} \quad \text{for } t \geq 0. \tag{16}$$

The total predicted transient circuit voltage can now be expressed as

$$\hat{u}_\tau = \hat{U}_1\,\mathrm{e}^{-\frac{t}{\tau_1}} + \hat{U}_2\,\mathrm{e}^{-\frac{t}{\tau_2}}. \tag{17}$$

For a model with *n*th order, generic expressions for the transient circuit voltage $u_{\tau_i}(t)$ as well as the time-constant $\hat{\tau}_i$, initial-voltage $\hat{U}_i$, and voltage $\hat{u}_i(t)$ predictions of the *i*th *RC* branch can be formulated as follows:

$$u_{\tau_i}(t) = \begin{cases} U_{\mathrm{oc}} - u_{\mathrm{b}}(t), & \text{if } i = n \\ U_{\mathrm{oc}} - u_{\mathrm{b}}(t) - \displaystyle\sum_{i+1}^{n} \hat{u}_{i+1}(t), & \text{if } i < n \end{cases} \tag{18}$$

$$\hat{\tau}_i = \frac{t_{i2} - t_{i1}}{\ln\left(\frac{u_{\tau_i}(t_{i1})}{u_{\tau_i}(t_{i2})}\right)}, \quad \text{for } u_{\tau_i} \neq 0 \tag{19}$$

$$\hat{U}_i = u_{\tau_i}(t_{i1})\,\mathrm{e}^{\frac{t_{i1}}{\hat{\tau}_i}} \tag{20}$$

$$\hat{u}_i(t) = \hat{U}_i\,\mathrm{e}^{-\frac{t}{\hat{\tau}_i}}, \quad \text{for } t \geq 0. \tag{21}$$

The resistance R_i and capacitance C_i values can be extracted with the knowledge of the preceding CP amplitude I_{cp} and duration t_{cp}, as follows:

$$R_i = \frac{\hat{U}_i}{I_{\mathrm{cp}}\left(1 - \mathrm{e}^{-\frac{t_{\mathrm{cp}}}{\hat{\tau}_i}}\right)} \tag{22}$$

$$C_i = \frac{\hat{\tau}_i}{R_i}. \tag{23}$$

In the above equations, the resistance and the time constant are assumed to be constant during the CP, which is obviously not true in general. However, the resulting inaccuracy in the parameter values causes only a negligible error in the voltage prediction. This issue can also be partly rounded by having a high number of CPs, e.g., 20, in the characterization experiment. However, the duration of the experiment increases, respectively, to the number of CPs and the duration of the rest period.

This parameter extraction method can be generalized to any number of *RC* branches as long as their time constants are well separated. The procedure goes always from the longest time-constant identification towards the shortest. There should also be a sufficiently long time gap between consecutive time windows to let the shorter time-constant branches voltages to drop into the vicinity of zero before the beginning of the next time window.

III. Experimental

A module-level test environment for battery characterization has been built in the laboratory (see Fig. 4). A commercial Li-ion polymer battery module from Kokam is investigated in

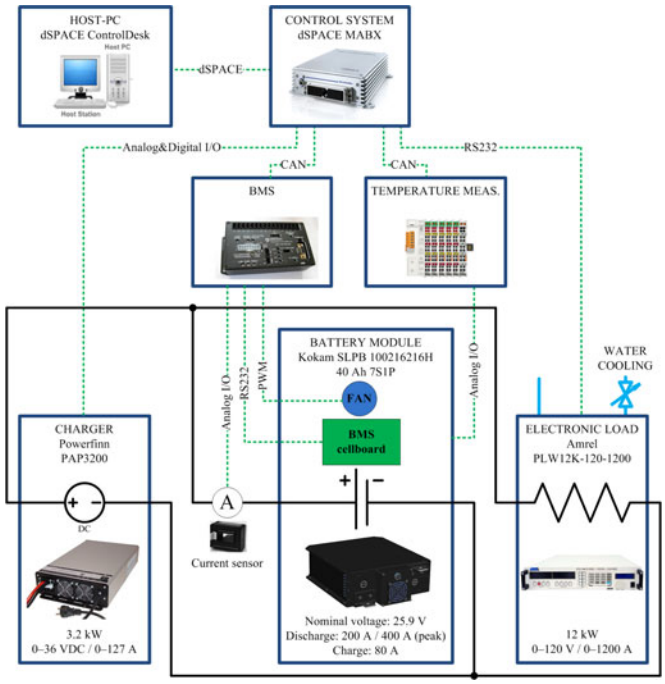

Fig. 4. Battery test setup. Also a power analyzer was used to measure battery terminal voltage, current, and ampere-hours.

TABLE I
SPECIFICATION OF THE BATTERY CELL AND MODULE

Property	Unit	Cell	Module
Nominal capacity	Ah	40	40
Nominal voltage	V	3.7	25.9
Max voltage	V	4.2	29.4
Cutoff voltage	V	2.7	18.9
Max charge current	A	80	80
Cont. discharge current	A	200	200
Peak discharge current	A	400	400

the experiments. The battery consists of seven series-connected SLPB 100216216H lithium-ion polymer pouch-type cells. The positive electrode material is lithium-nickel-manganese-cobalt-oxide and the negative electrode material is graphite. The specification of the battery is shown in Table I.

Load current is made with a water-cooled programmable dc electronic load, model PLW12K-120-1200 from Amrel, which has maximum current, voltage, and power ratings of 1 200 A, 120 V, and 12 kW, respectively. A Powerfinn PAP3200 is used as a power supply during charging. The power supply can be used as a controlled voltage or current source with output voltage area of 0–36 V and current area of 0–127 A. Its maximum output power is 3.2 kW at 24 V. A Hioki 3390 power analyzer with a Hioki 9278 current clamp is used to measure current, voltage, and ampere-hours.

All equipment except the power analyzer is controlled with a dSPACE MicroAutoBox (MABX) DS 1401/1505/1507 rapid control prototyping electronic control unit (ECU). Model-based software development is utilized to produce code for the ECU. Models are made with MATLAB/Simulink/Stateflow. The ECU is connected to the host computer via high-speed link. All measurements as well as other signals can be monitored online from the host computer through dSPACE ControlDesk software.

All relevant data are logged with 50-ms sampling interval. Data from ControlDesk and power analyzer are merged and postprocessed afterward to make a unified data structure that has all relevant information for battery characterization. For characterization and model validation, the power analyzer is considered to be more accurate and reliable source of data than the others, and hence, the power analyzer is used as the source of current, voltage, and ampere-hour data. Temperature data are obtained from ControlDesk.

Prior to starting the characterization, the battery was charged to its maximum voltage and the BMS balanced the cells to be in equal SOC. After the balancing was finished, the BMS was disabled, i.e., the balancing was set off and the BMS was not able to control the charger, the load, nor the contactors. Everything were controlled by the MABX and monitored from the host computer. The experiment was stopped when the first cell reached its cutoff voltage, i.e., 2.7 V.

Characterization of a battery module is more complicated than that of a single cell, because the cells are not identical but have slightly different capacities and resistances, and they may evolve differently when aging. Due to capacity differences, the capacity of a battery is determined by the cell with the lowest capacity. If all cells are fully charged at the beginning of a discharge test, only the weakest cell reaches the cutoff voltage. The average voltage curve does not reach the cutoff voltage. Also the shape of the voltage curve may differ from the ideal curve, because near the end-of-test (EOT) condition the cells are not in the same SOC. From a modeling perspective, this yields to a situation where the shape of the OCV curve of a battery pack may differ slightly from that of a single cell.

For high-fidelity modeling of a multicell battery, every cell should be modeled separately [19], [23]. The model of a battery can then be formed by connecting the cell models in appropriate series and parallel configuration [23]. However, this approach increases significantly the computational complexity of the model as well as parameter extraction effort, as the battery pack may consists of tens or hundreds battery cells in series and parallel connections. For system-level simulations, simplicity and light computational burden is often preferred. Hence, in this paper, the battery module was modeled as a single battery cell with the characteristics of the whole battery module. The resulting model characterizes the behavior of the module, but does not reveal accurate information about any of the cells. The module voltage can be divided by the number of cells to achieve the average value for cell voltage, OCV, and resistance and capacitance values.

IV. RESULTS

All experiments were made at room temperature. Inherent heating due to thermal losses was evident. The average temperature (T_{avg}) and temperature change (ΔT) of the experiments are presented in the end of this section together with the results

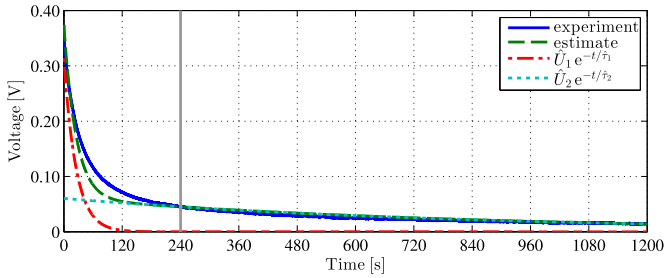

Fig. 5. Parallel *RC* circuit parameter extraction. Measured and estimated transient circuit voltage u_τ during the rest time. The vertical gray line marks the starting time of the second time window.

of the model validation. Unless otherwise stated, all temperature and error measures are for the SOC range of 10–100%.

A. Model Extraction

The capacity of the battery was measured to be approximately 45 Ah. For simplicity, the aging effects and self-discharge were ignored. A PD experiment with 1C rate, 10% pulse rate, and 30 min rest time was made to characterize the OCV and to extract base values for the ohmic resistance and *RC*-network parameters for discharge. Two *RC* circuits were used in the EEC, and the data were divided accordingly into sections. For simplicity, constant time windows were used: $t_{11} = 0$ s, $t_{12} = 12$ s, $t_{21} = 240$ s, and $t_{22} = 600$ s. However, below 10% SOC, the first time window was time-shifted for 5 s and lengthened to 15 s, i.e. $t_{11} = 5$ s, $t_{12} = 20$ s, to ensure correct behavior. This issue is further discussed later in this section. The resulting mean values of the time constants were 22 and 570 s. The parameter maps were upsampled by a factor of 10 with shape-preserving piecewise cubic interpolation method. This resulted in smoother parameter maps. Linear interpolation between data points were used in the simulations.

Fig. 5 illustrates the extraction procedure with an example. The figure shows the experimental transient circuit voltage data as well as the transient circuit voltage estimate of a model with two *RC* parallel branches during a rest time of 30 min. Also the predicted voltage of each *RC* branch as well as the starting time instant of the second time window are shown in the figure. The subtraction of the battery voltage from the OCV removes the final offset and inverts the voltage curve. Hence, the transient circuit voltage always decays from the initial voltage towards zero. It can be seen from the figure that the estimated voltage characterized the real behavior very well and that the condition for the separation of time windows was fulfilled.

After the PD test, a PC test was made to identify the parameters for charging. Then, PD and PC tests were made at 2C rate as well as at 4C rate for discharging. Two experiments (1C charge and 2C discharge) were made with 10-min rest time, while the others were made with 30-min rest time. The same time windows were used for all experiments. The resulting parameter mappings are presented in Fig. 6. No experiments at very low rates were done, because due to low current even a moderate error in parameter values causes only a minor error

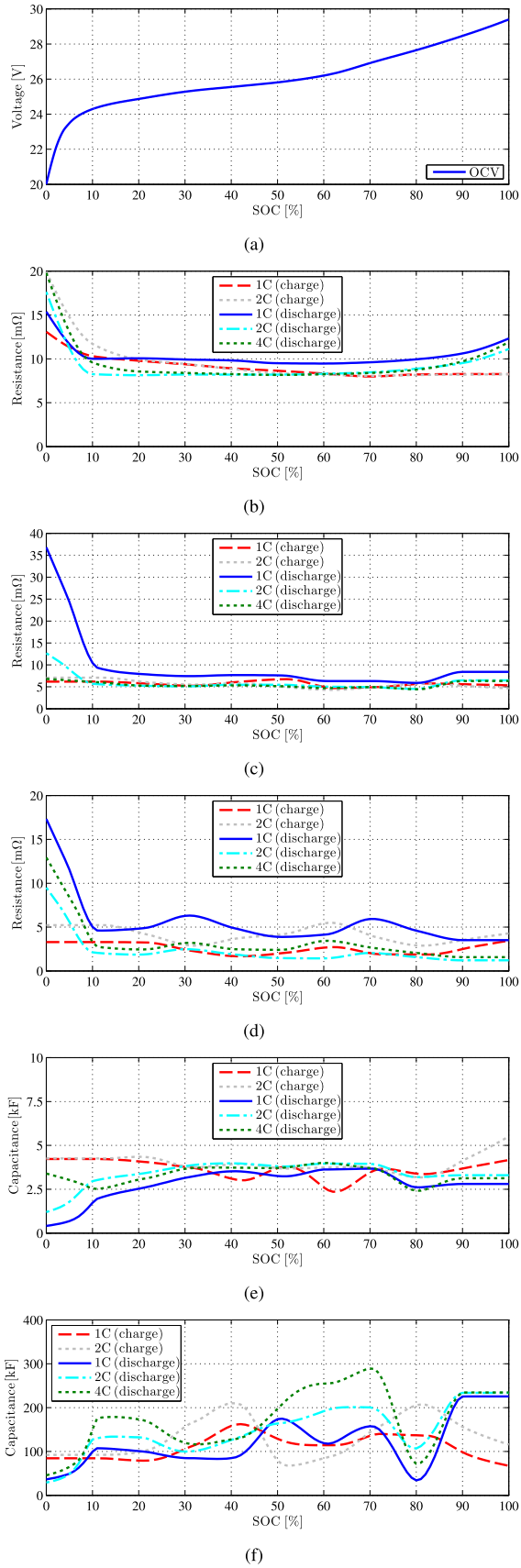

Fig. 6. Parameter mappings. (a) u_{oc}. (b) R_0. (c) R_1. (d) R_2. (e) C_1. (f) C_2.

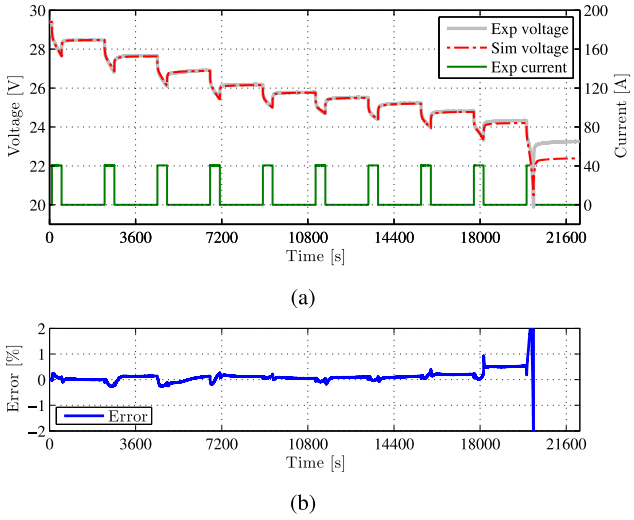

Fig. 7. PD experiment at 1C rate, 10% pulse rate, and 30 min rest time. (a) Measured and simulated voltage on the left axis and measured current on the right axis. (b) Voltage error.

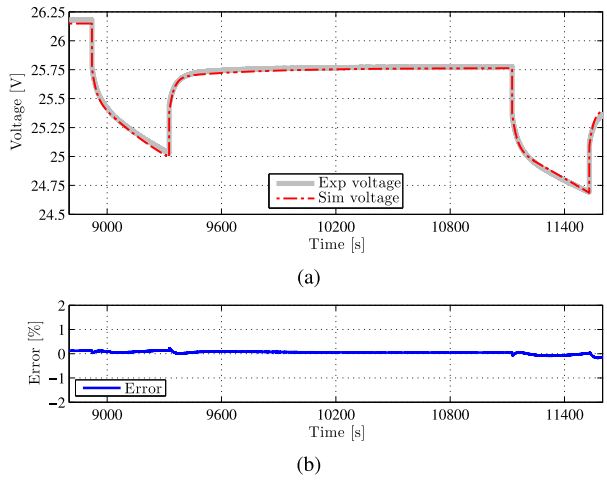

Fig. 8. Part of a PD experiment at 1C rate, 10% pulse rate, and 30 min rest time. (a) Measured and simulated voltage. (b) Voltage error. MAPE = 0.07%, RMSPE = 0.07%.

into the voltage prediction. It was also confirmed from the validation experiments that the voltage error during low-current periods remained very low, indicating that the parameter values are close to 1C-rate values.

The results of a PD experiment at 1C rate are shown in Figs. 7 and 8. The simulation results match very well with the experimental results. The mean absolute percentage error (MAPE) and root mean square percentage error (RMSPE) were 0.10% and 0.12%, respectively. The maximum absolute percentage error (APE) was 0.4%.

Below 10% SOC, the error during the transient increased to several percents, the maximum APE being 5.7%. The main reason for such a high error lies in the rapidly slowing dynamics of a battery when approaching fully discharged state. This starts to happen at SOC level of 10–20% [13]. Two *RC* circuits cannot

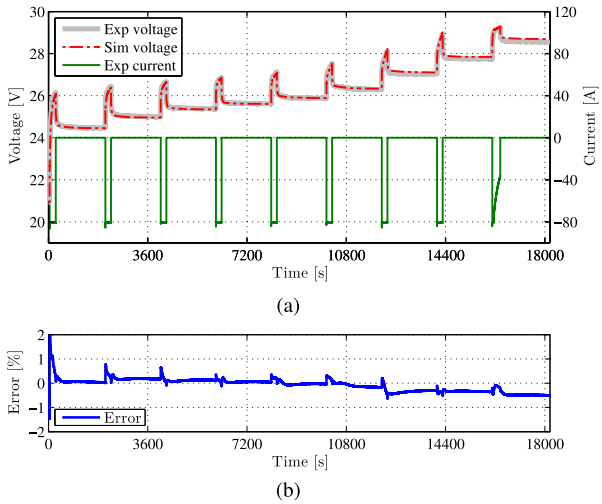

Fig. 9. PC experiment at 2C rate, 10% pulse rate, and 30 min rest time. (a) Measured and simulated voltage on the left axis and measured current on the right axis. (b) Voltage error.

anymore characterize the real behavior, but a third *RC* circuit would be needed to represent the second-scale time constant. This second-scale resistance increases very rapidly and captures a high voltage. With only two *RC* branches, this resistance should not be included in neither of the *RC* branches. This can be ensured in the model extraction algorithm by shifting the time windows at low SOC further from the beginning of the rest period, i.e., by selecting t_{11} to be something like 5 s, and if needed, the other time instants time-shifted as well. It would be possible to include the second-scale resistance partly or fully into the ohmic resistance R_0. However, then, the ohmic resistance R_0 of the model would not represent a pure ohmic resistance anymore. Therefore, for clarity, the second-scale resistance was ignored.

It can also be seen from the figure that the OCV at the EOT is inaccurate, which is caused by the inaccuracies in the SOC prediction and OCV mapping. Even small inaccuracies get visible below 10% SOC, because of the high nonlinearity and steep slope of the OCV-curve.

The results of a PC experiment at 2C rate, PD experiment at 4C rate, and a constant-current discharge (CCD) experiment at 1C rate are shown in Figs. 9–11, respectively.

B. Model Validation

The model was validated using a measured power profile of an underground mining load-haul-dump (LHD) loader [24]. The power profile is shown in Fig. 12. The validation current profile has short-time current peaks with different amplitudes as well as constant-current periods, and thus, is a good profile for validation purposes in general.

The average power of the cycle was 30 kW. A series-hybrid topology with a battery in the dc link was considered. The internal combustion engine (ICE) operates with constant power of 25 kW, and thus, the power profile of the battery was obtained by moving the power profile of Fig. 12 downwards 25 kW. Since the ICE power was less than the average power of the duty cycle,

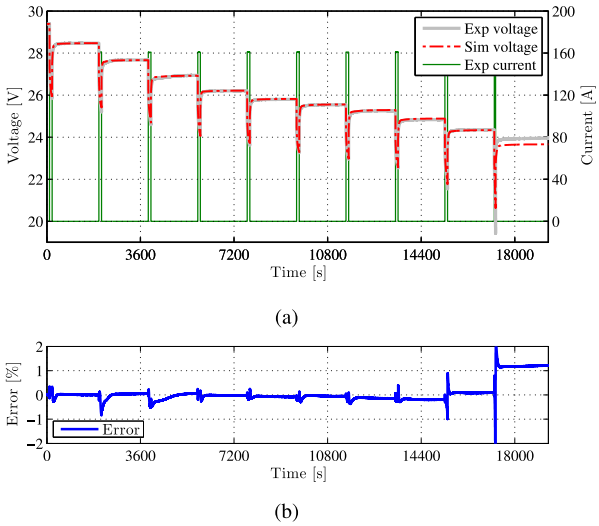

Fig. 10. PD experiment at 4C rate, 10% pulse rate, and 30 min rest time. (a) Measured and simulated voltage on the left axis and measured current on the right axis. (b) Voltage error.

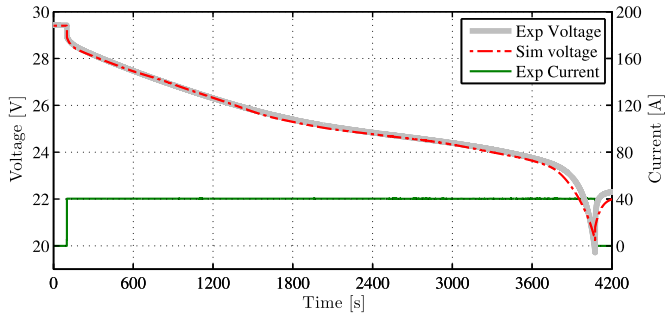

Fig. 11. CCD experiment at 1C rate. Measured and simulated voltage on the left axis and measured current on the right axis.

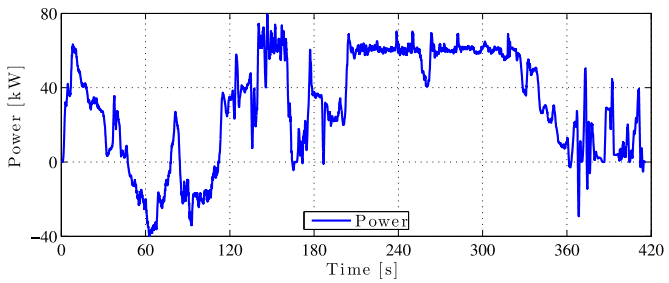

Fig. 12. Duty cycle of an underground mining LHD loader.

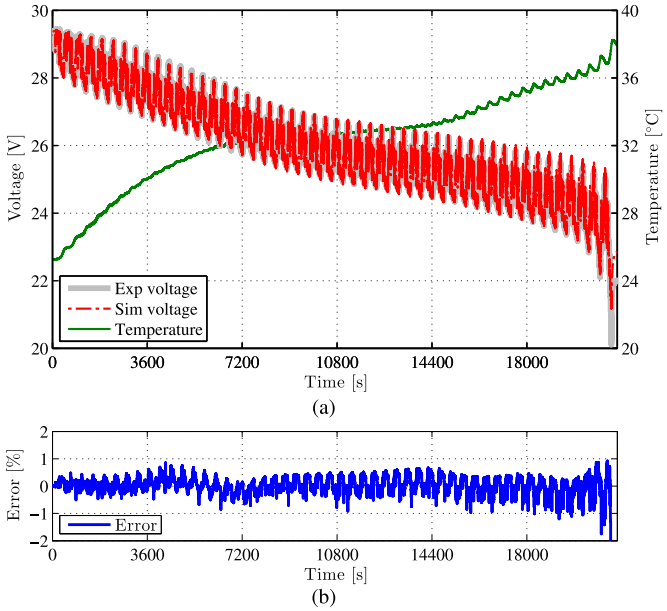

Fig. 13. Model validation, LHD cycle repeated until cell cutoff voltage is reached. (a) Measured and simulated voltage on the left axis and measured temperature on the right axis. (b) Voltage error.

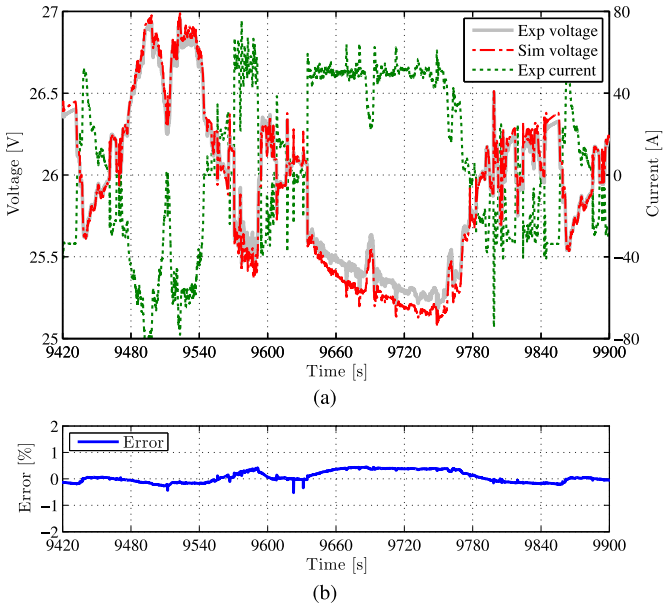

Fig. 14. Model validation, approximately one LHD cycle in the middle of the experiment. (a) Measured and simulated voltage on the left axis and measured current on the right axis. (b) Voltage error. MAPE = 0.18%, RMSPE = 0.23%.

the considered cycle represented a charge depleting cycle with approximately 2% decrement in SOC per cycle. The power was scaled down with a factor of 28 to represent the power of a single battery module. The battery current was calculated in real-time in the MABX ECU based on the measured battery module voltage. The result of the validation experiment is shown in Fig. 13 and a part of the full test is shown in Fig. 14 to show details during one cycle.

The average temperature, temperature change, and error measures of the experiments are shown in Table II. Typically the temperature rose in the beginning and in the end and had a plateau in the middle of the experiment, where the temperature stayed within 5 °C for a length of over 50% of the full capacity. The results show that with a second-order model less than 0.3% MAPE and 0.4% RMSPE for voltage prediction at SOC range of 10–100% was achieved despite the non-isothermal conditions. It can be deduced that the presented parameter extraction method performs well. Temperature scheduling and better thermal stability would further increase the accuracy.

TABLE II
TEMPERATURE AND ERROR CHARACTERISTICS, SOC RANGE: 10–100%

Experiment	T_{avg}	ΔT	Max APE	MAPE	RMSPE
PD 1C / 30 min	27 °C	7 °C	0.4%	0.10%	0.12%
PD 2C / 10 min	34 °C	14 °C	0.8%	0.18%	0.24%
PD 4C / 30 min	34 °C	17 °C	1.0%	0.10%	0.14%
PC 1C / 10 min	31 °C	4 °C	0.7%	0.20%	0.22%
PC 2C / 30 min	32 °C	9 °C	0.8%	0.20%	0.25%
CCD 1C	29 °C	11 °C	0.8%	0.28%	0.32%
LHD	32 °C	11 °C	1.2%	0.22%	0.27%

V. CONCLUSION

The presented parameter extraction method is based on the analysis of voltage relaxation characteristics of experimental PD and PC tests. This provides a rapid analytical method to characterize all necessary model parameters offline from experimental voltage data without a need to optimize the parameters iteratively by simulating the system and updating the parameters. The method can be used to extract parameters for any number of *RC* branches. The model extraction experiments are easy to program and execute and the parameterization process can be fully automated.

Future work will focus on more detailed investigations on the temperature and rate effects.

REFERENCES

[1] M. S. Whittingham, "History, evolution, and future status of energy storage," *Proc. IEEE*, vol. 100, pp. 1518–1534, May 2012.

[2] B. Pattipati, C. Sankavaram, and K. R. Pattipati, "System identification and estimation framework for pivotal automotive battery management system characteristics," *IEEE Trans. Syst., Man, Cybern. C, Appl. Rev.*, vol. 41, no. 6, pp. 869–884, Nov. 2011.

[3] N. Chaturvedi, R. Klein, and J. Christensen, "Algorithms for advanced battery-management systems," *IEEE Control Syst. Mag.*, vol. 30, no. 3, pp. 49–68, Jun. 2010.

[4] P. Rong and M. Pedram, "An analytical model for predicting the remaining battery capacity of lithium-ion batteries," *IEEE Trans. Very Large Scale Integr. Syst.*, vol. 14, no. 5, pp. 441–451, May 2006.

[5] S. Barsali and M. Ceraolo, "Dynamical models of lead-acid batteries: Implementation issues," *IEEE Trans. Energy Convers.*, vol. 17, no. 1, pp. 16–23, Mar. 2002.

[6] M. Chen and G. A. Rincón-Mora, "Accurate electrical battery model capable of predicting runtime and *I-V* performance," *IEEE Trans. Energy Convers.*, vol. 21, no. 2, pp. 504–511, Jun. 2006.

[7] S. Buller, M. Thele, R. W. A. A. D. Doncker, and E. Karden, "Impedance-based simulation models of supercapacitors and Li-ion batteries for power electronic applications," *IEEE Trans. Ind. Appl.*, vol. 41, no. 3, pp. 742–747, May/Jun. 2005.

[8] T. Kim and W. Qiao, "A hybrid battery model capable of capturing dynamic circuit characteristics and nonlinear capacity effects," *IEEE Trans. Energy Convers.*, vol. 26, no. 4, pp. 1172–1180, Dec. 2011.

[9] X. Hu, S. Li, and H. Peng, "A comparative study of equivalent circuit models for Li-ion batteries," *J. Power Sources*, vol. 198, pp. 359–367, 2012.

[10] N. Watrin, R. Roche, H. Ostermann, B. Blunier, and A. Miraoui, "Multiphysical lithium-based battery model for use in state-of-charge determination," *IEEE Trans. Veh. Technol.*, vol. 61, no. 8, pp. 3420–3429, Oct. 2012.

[11] H. He, R. Xiong, X. Zhang, F. Sun, and J. Fan, "State-of-charge estimation of the lithium-ion battery using an adaptive extended Kalman filter based on an improved Thevenin model," *IEEE Trans. Veh. Technol.*, vol. 60, no. 4, pp. 1461–1469, May 2011.

[12] B. Schweighofer, K. M. Raab, and G. Brasseur, "Modeling of high power automotive batteries by the use of an automated test system," *IEEE Trans. Instrum. Meas.*, vol. 52, no. 4, pp. 1087–1091, Aug. 2003.

[13] S. Abu-Sharkh, and D. Doerffel, "Rapid test and non-linear model characterisation of solid-state lithium-ion batteries," *J. Power Sources*, vol. 130, pp. 266–274, 2004.

[14] J. Li, M. Mazzola, J. Gafford, and N. Younan, "A new parameter estimation algorithm for an electrical battery model," in *Proc. Appl. Power Electron. Conf.*, Orlando, FL, USA, Feb. 2012, pp. 427–433.

[15] B. Schweighofer, H. Wegleiter, M. Recheis, and P. Fulmek, "Fast and accurate battery model applicable for EV and HEV simulation," in *Proc. IEEE Int. Instrum. Meas. Technol. Conf.*, May 2012, pp. 565–570.

[16] D. V. Do, C. Forgez, K. E. K. Benkara, and G. Friedrich, "Impedance observer for a Li-ion battery using Kalman filter," *IEEE Trans. Veh. Technol.*, vol. 58, no. 8, pp. 3930–3937, Oct. 2009.

[17] T. Hu, B. Zanchi, and J. Zhao, "Simple analytical method for determining parameters of discharging batteries," *IEEE Trans. Energy Convers.*, vol. 26, no. 3, pp. 787–798, Sep. 2011.

[18] X. Hu, F. Sun, Y. Zou, and H. Peng, "Online estimation of an electric vehicle lithium-ion battery using recursive least squares with forgetting," in *Proc. Amer. Control Conf.*, San Francisco, CA, USA, Jun./Jul. 2010, pp. 935–940.

[19] M. A. Roscher, O. S. Bohlen, and D. U. Sauer, "Reliable state estimation of multicell lithium-ion battery systems," *IEEE Trans. Energy Convers.*, vol. 26, no. 3, pp. 737–743, Sep. 2011.

[20] Y. Hu, S. Yurkovich, Y. Guezennec, and B. Yurkovich, "A technique for dynamic battery model identification in automotive applications using linear parameter varying structures," *Control Eng. Pract.*, vol. 17, pp. 1190–1201, 2009.

[21] M. Einhorn, F. V. Conte, C. Kral, and J. Fleig, "Comparison, selection and parameterization of electrical battery models for automotive applications," *IEEE Trans. Power Electron.*, vol. 28, no. 3, pp. 1429–1437, Mar. 2013.

[22] D. Linden, *Linden's Handbook of Batteries*, T. B. Reddy, Ed., 4th ed. New York, NY, USA: McGraw-Hill, 2011.

[23] J. Zhang, S. Ci, H. Sharif, and M. Alahmad, "Modeling discharge behavior of multicell battery," *IEEE Trans. Energy Convers.*, vol. 25, no. 4, pp. 1133–1141, Dec. 2010.

[24] T. Lehmuspelto, M. Heiska, A. Leivo, and A. Hentunen. (2009). Hybridization of a mobile work machine, *World Electric Veh. J.* [Online]. *3*. Available: http://www.evs24.org/wevajournal

Ari Hentunen (M'10) received the M.Sc. (Tech.) degree from the Helsinki University of Technology, Espoo, Finland, in 2005, and the Lic.Sc. (Tech.) degree from Aalto University (formerly Helsinki University of Technology), Espoo, in 2012. He is currently working toward the D.Sc. (Tech.) degree at the Aalto University.

His main research interests include modeling of lithium-ion batteries and control of hybrid electric vehicles.

Teemu Lehmuspelto (M'04) received the M.Sc. degree in mechanical engineering from the Helsinki University of Technology, Espoo, Finland, in 2001.

From 2001 to 2008, he was an R&D Engineer at Patria Land & Armament Oy. Since 2008, he has been a Research Scientist at the Aalto University (formerly Helsinki University of Technology), Espoo. His main research interests include vehicle control technologies and hybrid electric vehicle technologies.

Jussi Suomela received the M.Sc., Lic.Sc., and D.Sc. degrees from the Helsinki University of Technology, Espoo, Finland, in 1992, 2001, and 2004, respectively.

From 1991 to 2012, he was with the Helsinki University of Technology (part of Aalto University, Espoo, since 2010). From 2010 to 2012, he was an Acting Professor of automation technology. Since 2012, he has been working at Hybria Oy, Espoo. His main research interests include hybrid electric transmission in off-road mobile machines and field and service robotics.